Mon. Not. R. astr. Soc. (1984) **210,** 929–951

The bridges of classical double radio sources

J. P. Leahy and A. G. Williams *Mullard Radio Astronomy Observatory, Cavendish Laboratory, Madingley Road, Cambridge CB3 0HE*

Accepted 1984 May 9. Received 1984 May 8; in original form 1984 January 12

Summary. New observations with the VLA of a complete sample of 39 3C sources with angular sizes larger than 45 arcsec are discussed. Nearly all of the classical double sources at redshifts less than 0.5 have bridges linking the central galaxy with the outer edge of the source, and our maps of these objects show that two-thirds of the bridges are significantly distorted near the central galaxy. Such distortions may be predicted from the jet model for double radio sources if the jet is much lighter than the confining medium, since the dynamics of the bridge region are then dominated by backflow of material that has passed through the hotspots. There is a correlation between axial ratio and luminosity which may be physically related to the compactness relation of Jenkins & McEllin.

1 Introduction

The low-surface-brightness 'tails' and 'bridges' of extragalactic radio sources have in the past been difficult to observe because of the presence of the intense hotspots, and the consequent need for very large dynamic ranges on maps with the arcsecond beamwidths required to resolve the bridge transversely. With the advent of the VLA these conditions can now be met, and we have used it to map a sample of extended radio galaxies to study their bridges in total intensity and polarization. Here we present the total intensity observations of the classical double sources (in classes I–II and II of Fanaroff & Riley 1974, hereafter FR), and discuss them in relation to numerical simulations of supersonic jets. We assume $H_0=100\,\mathrm{km\,s^{-1}\,Mpc^{-1}}$ and $q_0=0$ throughout.

2 The sample

The sources discussed are drawn from a complete sample covering about 2 sr defined by $S_{178}\geqslant 10$ Jy, $45\leqslant\theta\leqslant 600$ arcsec, $\delta>10°$, $b>50°$, or $|b|<10°$, and containing 39 sources. θ is defined as the largest angular size, rather than the distance between the outer peaks of emission. The criteria for definition of the sample will be discussed in a later paper (Leahy, Pooley & Riley, in preparation). The sources with $b>50°$ are a subset of the sample discussed by Laing, Riley & Longair (1983, hereafter LRL), while those with $|b|<10°$ were selected by an analogous procedure. Eight of the sources are of head-tail or twin-jet type (class I of FR) and are not

Table 1. The sample.

Source	S_{178}	θ	z	Log(P)	D	Dist	R_N	R_S	R_T
4C 60.02	13.2	56	-	-	-	1	8.2*	4.8*	12.2
3C 52	13.5	51	(0.2)	25.6	115	3	5.0	4.0	8.8
3C 69	20.9	48	-	-	-	1	3.1	4.9*	8.0
3C 103	26.6	88	(0.2)	25.9	195	1	5.8	5.4	11.2
3C 111	64.6	275	0.0485	25.13	181	5	1.75	1.1	2.8
3C 134	74.4	136	-	-	-	3	3.2	5.6	8.0
3C 136.1	14.0	415	0.0640	24.71	352	3	2.1	3.8	5.8
3C 139.2	11.9	138	-	-	-	2	8.4	9.9*	18.2
3C 165	13.5	87	(0.3)	26.1	260	4	1.9	2.3	4.2
3C 166	14.7	45	0.2490	25.99	117	1	2.1	2.1	4.2
3C 234	31.4	110	0.1848	26.03	230	4	5.7	4.2	10.0
3C 244.1	20.3	53	0.4280	26.64	196	1	5.7*	5.0*	10.6
3C 274.1	16.5	150	0.4220	26.55	551	3	4.4	4.7	9.0
3C 284	11.3	175	0.2394	25.84	444	2	5.1	3.6	8.6
3C 285	11.3	134	0.0794	24.82	138	4	1.5	2.5	3.4
3C 293	12.7	216	0.0452	24.36	133	-	-	-	-
3C 300	17.9	100	0.2700	26.13	276	2	4.9	1.8	6.6
3C 310	55.1	310	0.0540	25.16	225	5	1.3	1.1	2.4
3C 315	17.8	200	0.1083	25.29	270	3	4.0	3.2	7.2
3C 319	15.3	105	0.1920	25.76	226	4/5	2.1	5.5	6.4
3C 321	13.5	290	0.0960	25.05	353	-	-	-	-
3C 399.1	13.5	54	-	-	-	1	4.5*	5.5*	9.8
3C 405	8700.0	106	0.0565	27.39	80	2	4.3	5.5	9.8
3C 430	33.7	85	0.0541	24.94	62	5	1.5	2.2	3.6

Key to Table 1:
S_{178}: Flux at 178 MHz. θ: Largest angular size.
z: Redshift. Log(P): log of Power at 178 MHz.
D: Largest projected size. Dist: Distortion (see Table 5).
R_N: Axial ratio of Northern bridge. R_S: Axial ratio of Southern bridge.
R_T: Average axial ratio of source.

An asterisk follows R values where the deconvolved half-power width of the bridge was less than 1.5 HPBWs.

relevant to the present discussion. The remaining 31 have each been observed with similar resolution and sensitivity (see below). Of these, five are distant, high-luminosity sources ($z>0.5$, $P_{178}>10^{27}$ W Hz^{-1} sr^{-1}) in which no bridge emission is discernible. This is expected from the correlation between luminosity and the compactness parameter of Jenkins & McEllin (1977). Two unidentified sources have similar structures and are presumably similarly distant. Removing these seven sources is equivalent to imposing a redshift limit $z\lesssim0.5$. Table 1 gives various parameters (discussed in Section 5) for the resulting sample of 24 objects; Table 2 lists the 15 excluded sources. Eighteen of the sources in the final sample are identified with galaxies, one with a possible galaxy, and the remaining five (all close to the Galactic plane) are unidentified. As usual for a flux-density-limited sample there is a strong correlation between redshift and luminosity, but the redshift cut-off means that cosmological evolution has little effect on the sample. Fig. 1 plots P_{178} against linear size D for the sample, together with the angular-size limits for sources at the flux-density limit. For reference, we also plot the median linear size as a function of luminosity for the extended sources in the LRL sample. Although our angular size limits introduce some correlation between P and D, about 2/3 of all FR II sources with $z<0.5$ are in the angular size range considered.

Table 2. Rejected sources.

Source	Reason	Source	Reason
3C 27	High-P structure	3C 272.1	FR I
3C 129	FR I	1227+119	FR I
3C 129.1	FR I	3C 274	FR I
3C 130	FR I	3C 277.2	z > 0.5
3C 154	z > 0.5	3C 292	z > 0.5
3C 252	z > 0.5	3C 296	FR I
3C 264	FR I	3C 428	High-P structure
3C 265	z > 0.5		

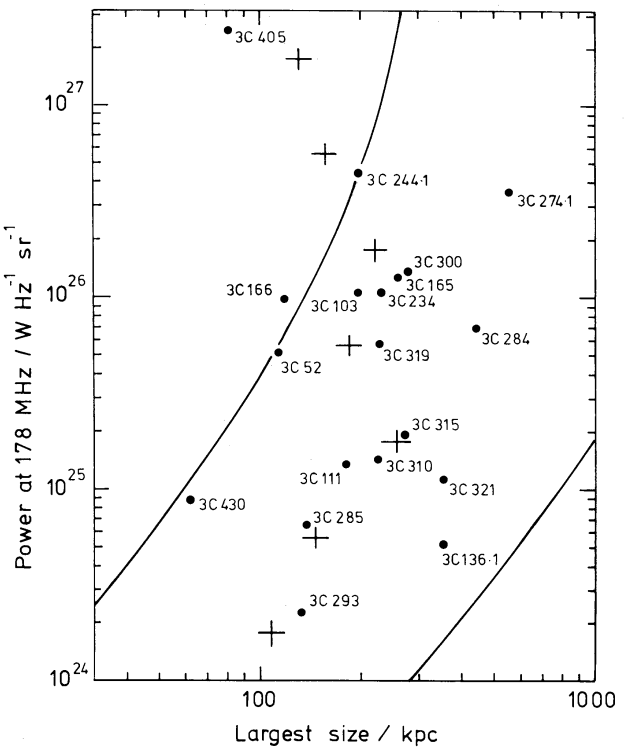

Figure 1. Plot of radio power at 178 MHz against the largest projected linear size for the sources discussed. The curves give the locus of 10 Jy sources at angular sizes 45 and 600 arcsec. Sources lying outside the region boundary by the lines are unlikely to have been included. The crosses give the median linear size of extended source in the LRL sample, in luminosity bins width 0.5 in log (P).

While it might be expected that a sample selected at a higher frequency would contain fewer sources with strong bridges, examination of the 2.7-GHz sample of Peacock & Wall (1981) shows that this is not the case, since all their sources in the relevant ranges of angular size, redshift, and morphology appear also in the LRL sample. There is thus no evidence for any substantial population of FR II sources without bridges excluded by our relatively low selection-frequency.

3 Observations and data reduction

The VLA is described by Thompson *et al.* (1980). All sources were observed at 18 and 21 cm with the VLA 'B' configuration in 'multiple snapshot' mode. For the larger sources, further snapshot observations in the 'C' configuration were made to complete the aperture coverage for the large-scale structure. Details of the observing runs are given in Table 3. All sources were expected to be unresolved on the shortest baseline, except for 3C 136.1, which is only slightly resolved.

Table 3. VLA observations.

Configuration	B	C
Date	September 1982	February 1983
Frequencies / MHz	1411 1646	1417 1652
Bandwidth / MHz	25	25
Calibrators	0212+735 3C 138 3C 286 1123+264 1252+119 1347+539 1511+238 2055+508 NRAO 140	3C 119 3C 138 3C 286 0552+398 1252+119 1504+377 1511+238
Flux density Standards	0212+735, 3C 286	
Flux density Scale	Baars et al (1977)	

Table 4. Data for maps.

Source	No. Scans B	C	RA	HPBW DEC arcsec	Ref
4C 60.02	2	-	4.5	4.0	-
3C 52	2	-	4.0	4.0	-
3C 69	2	-	4.2	4.2	PH
3C 103	2	-	3.7	3.7	-
3C 111 *	2	3	10.0	10.0	JPR
3C 134	2	3	4.5	4.5	-
3C 136.1	2	4	10.0	10.0	-
3C 139.2	2	4	4.1	4.4	-
3C 165	2	-	3.8	3.8	-
3C 166	2	-	3.8	3.8	SB
3C 234 *	2	2	4.0	5.7	RP
3C 244.1	2	-	3.75	3.75	JPR
3C 274.1	2	3	4.5	4.5	JPR
3C 284	3	2	5.0	5.0	RP
3C 285	2	2	5.0	5.5	-
3C 293 *	3	2	5.1	7.6	BFC
3C 300 *	2	-	4.4	4.4	RP
3C 310	2	2	10.0	10.0	vBF
3C 315	2	2	5.5	5.5	-
3C 319	2	-	4.0	4.0	BF
3C 321 *	2	2	6.0	7.0	JPR
3C 399.1	1	-	4.5	3.9	-
3C 405 *	2	-	5.4	5.4	S
3C 430 *	2	-	5.3	3.5	RP

Note: the source name is followed by a star if the map has been self-calibrated for amplitudes.

References:

BF	Bridle & Fomalont (1979)
BFC	Bridle, Fomalont, & Cornwell (1981)
JPR	Jenkins, Pooley, & Riley (1977)
PH	Pooley & Henbest (1974)
RP	Riley & Pooley (1975)
S	Scott (1982)
SB	Spangler & Bridle (1982)
vBF	van Breugel & Fomalont (1984)

Typically, two snapshots were made in each configuration, in well-separated hour angles with about 5-min integration each in the B configuration, and 4-min each in the C configuration. Calibration followed normal VLA practice, with calibration sources observed approximately hourly. Further observational details on individual sources are given in Table 4.

Subsequent reduction was performed with the AIPS system (Fomalont & Bridle 1983) at the VLA. After initial mapping and cleaning, all sources were self-calibrated for phase using the clean-component driven algorithm of Schwab (1980). For those sources dominated by very intense components, further iterations of the map/clean/self-cal cycle were performed, with amplitude as well as phase being calibrated on the final cycle. Care was taken to include in the self-cal solution those baselines reasonably well modelled by the clean-component image. For a few of the most extended sources, the aperture plane was under-sampled at the longer baselines so a Gaussian weighting was applied to the aperture plane, reducing the resolution until the images were dominated by densely-sampled shorter baselines.

The final clean maps were restored with elliptical Gaussian beams oriented in pa 0° or 90° to facilitate later multifrequency comparison. Dynamic ranges for the maps (defined as peak brightness/rms noise) are between 2000 and 100. Our maps are the most sensitive available at arcsec resolution for nearly all our sources. References to higher resolution maps (mostly from the Cambridge 5-km telescope at 5 GHz) are given in Table 4.

4 The maps

Contour maps of 24 sources are presented in Fig. 2. The contours are linear in each case, but the contour interval is occasionally changed to prevent overcrowding and peak contours are

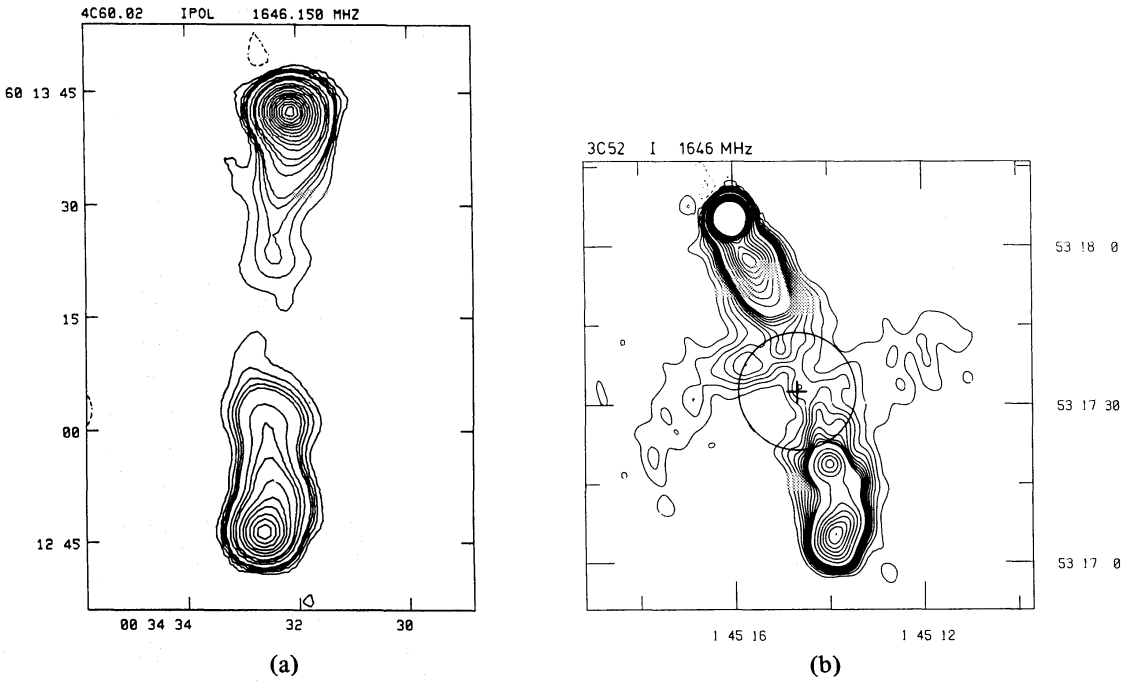

Figure 2. Contour maps. In each map a circle of 25-kpc radius is drawn around the galaxy centre. Negative contours are shown dashed. For each map we list the source name, the peak brightness in Jy/beam; and the contour levels in mJy/beam. In the contour lists, an ellipsis (. . .) indicates repetition of the same interval. Occasionally, the smallest negative contour requested was below the map minimum. In these cases, this contour level is also listed to indicate the reliability of the map.

(a) 4C60.02. Peak 0.693. Contours at −3, 3, 6, . . . 15, 30, . . . 60, 100, 140, 180, 240, . . . 660.
(b) 3C52. Peak 1.17. Contours at −6, −3, 3, 6, . . . 30, 50, . . . 250.
(c) 3C69. Peak 0.726. Contours at −5, 5, 10, . . . 30, 60, . . . 150, 300, 450, 600.
(d) 3C103. Peak 1.39. Contours at −12, −8, −4, 4, 8, . . . 40, 60, 80, 100, 150, . . . 300.
(e) 3C111. Peak 2.15. Contours at −5, 5, 10, . . . 30, 40, . . . 100, 150, . . . 400, 500, . . . 1000.
(f) 3C134. Peak 0.323. Contours at −2, 2, 6, 10, . . . 30, 40, . . . 130.
(g) 3C136.1. Peak 0.141. Contours at −1, 1, 3, 5, . . . 15, 20, . . . 50, 60, 70, 80.
(h) 3C139.2. Peak 0.270. Contours at −1.5, 1.5, 3, . . . 15, 20, . . . 50, 75, . . . 275.
(i) 3C165. Peak 0.098. Contours at −3, 3, 6, . . . 30, 40, . . . 90.
(j) 3C166. Peak 0.429. Contours at −5, 5, 10, . . . 50, 60, . . . 150, 200, . . . 400.
(k) 3C234. Peak 1.22. Contours at −6, 6, 12, . . . 90, 120, . . . 300, 450, . . . 1200.
(l) 3C244.1. Peak 1.25. Contours at −5, 5, 10, . . . 30, 60, . . . 150, 300, . . . 1200.
(m) 3C274.1. Peak 0.202. Contours at −2, 2, 4, . . . 20, 25, . . . 50, 60, 70, 80.
(n) 3C284. Peak 0.274. Contours at −2, 2, 4, . . . 10, 15, . . . 40, 50, . . . 100.
(o) 3C285. Peak 0.029. Contours at −2, 2,4, . . . 28.
(p) 3C293. Peak 3.45. Contours at −5, 5, 10, . . . 50, 60, . . . 130.
(q) 3C300. Peak 0.868. Contours at −4, 4, 8, . . . 20, 30, . . . 100, 120, . . . 200.
(r) 3C310. Peak 0.121. Contours at −2, 2, 4, . . . 12, 16, . . . 64.
(s) 3C315. Peak 0.317. Contours at −2, 2, 6, 10, 14, . . . 50, 60, . . . 110.
(t) 3C319. Peak 0.126. Contours at −2, 2, 4, . . . 10, 15, . . . 40, 50, . . . 80, 100, 120.
(u) 3C321. Peak 1.21. Contours at −6, −3, 3, 6, . . . 15, 30, 40, 50, 75, 100, . . . 200, 400, . . . 1000.
(v) 3C399.1. Peak 0.951. Contours at −5, 5, 10, . . . 30, 60, . . . 150, 300, . . . 900.
(w) 3C405. Peak 108. Contours (Jy) at −2, 2, 4, . . . 10, 15, . . . 30, 40, . . . 100.
(x) 3C430. Peak 0.433. Contours at −10, 10, 20, . . . 100, 120, . . . 200, 250, . . . 400.

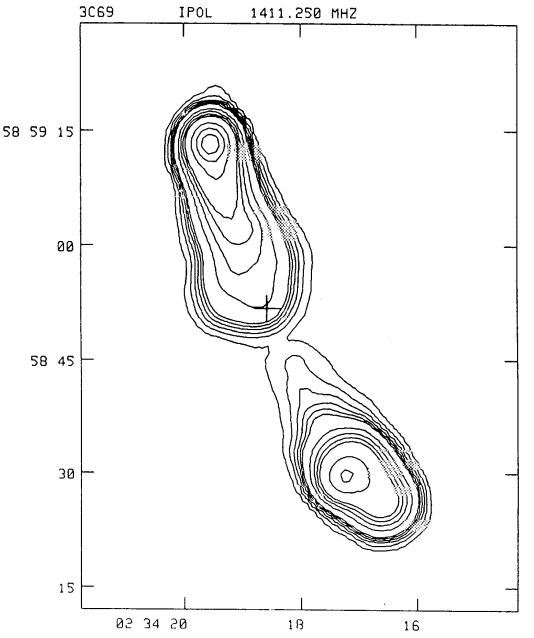

(c)

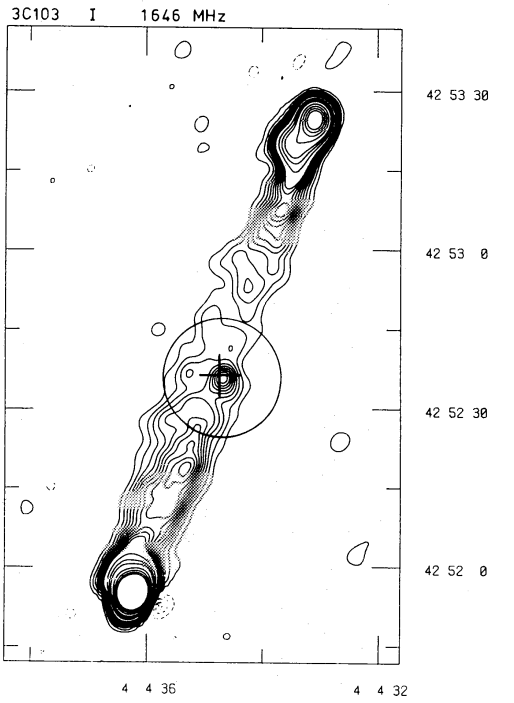

(d)

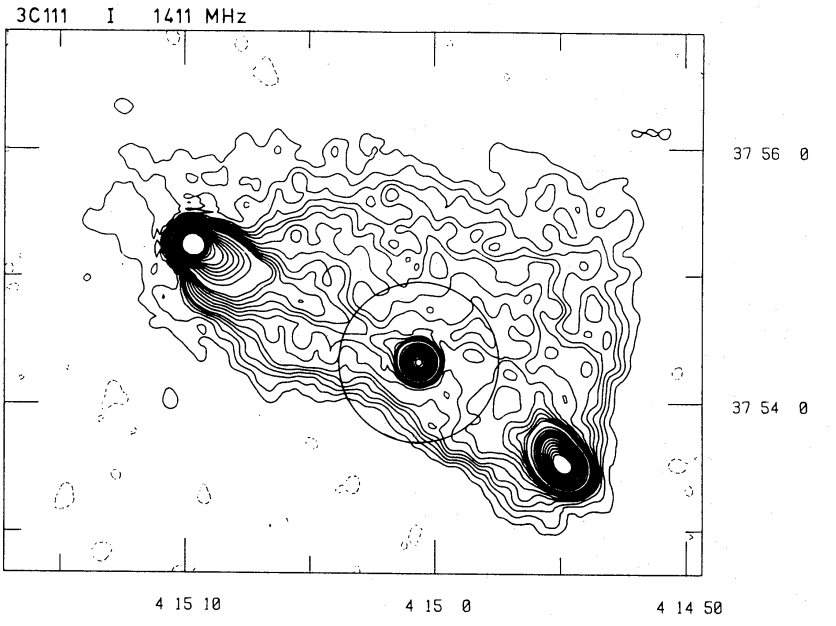

(e)

Figure 2 – *continued*

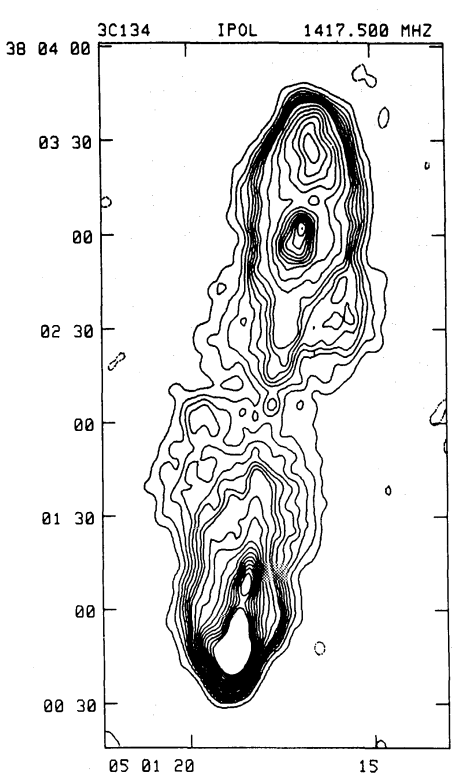

(f)

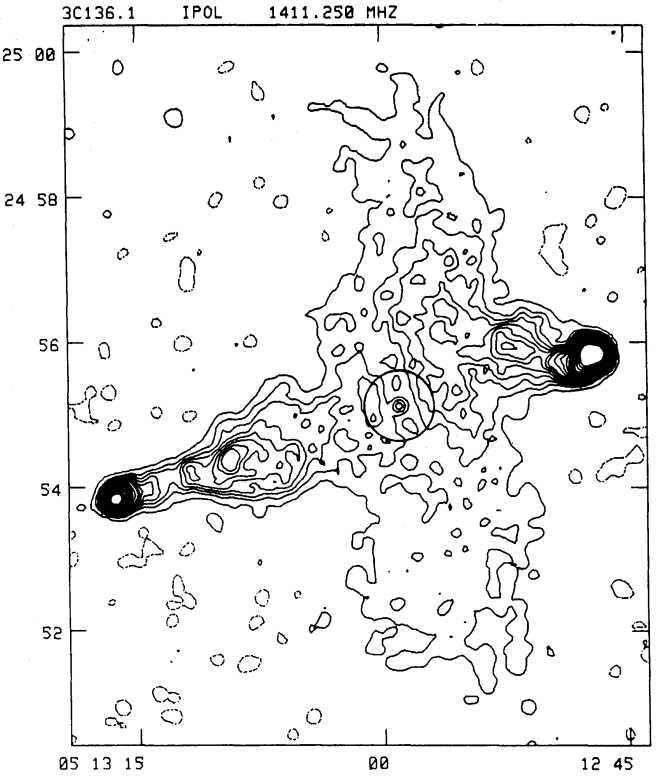

(g)

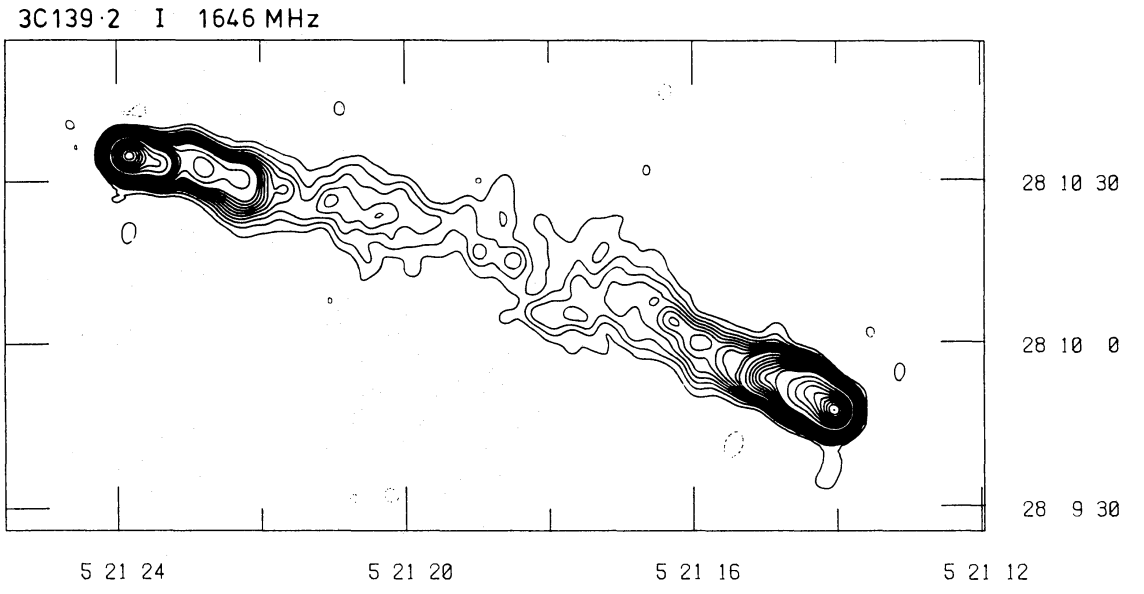

(h)

Figure 2 – *continued*

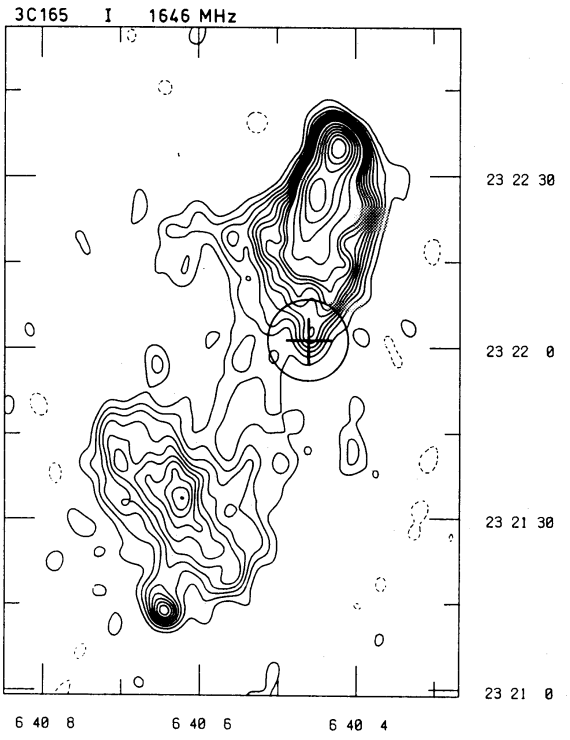

(i)

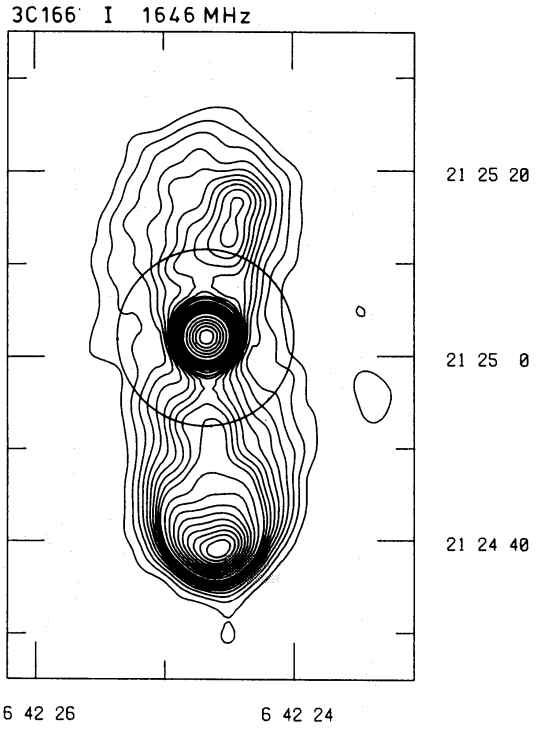

(j)

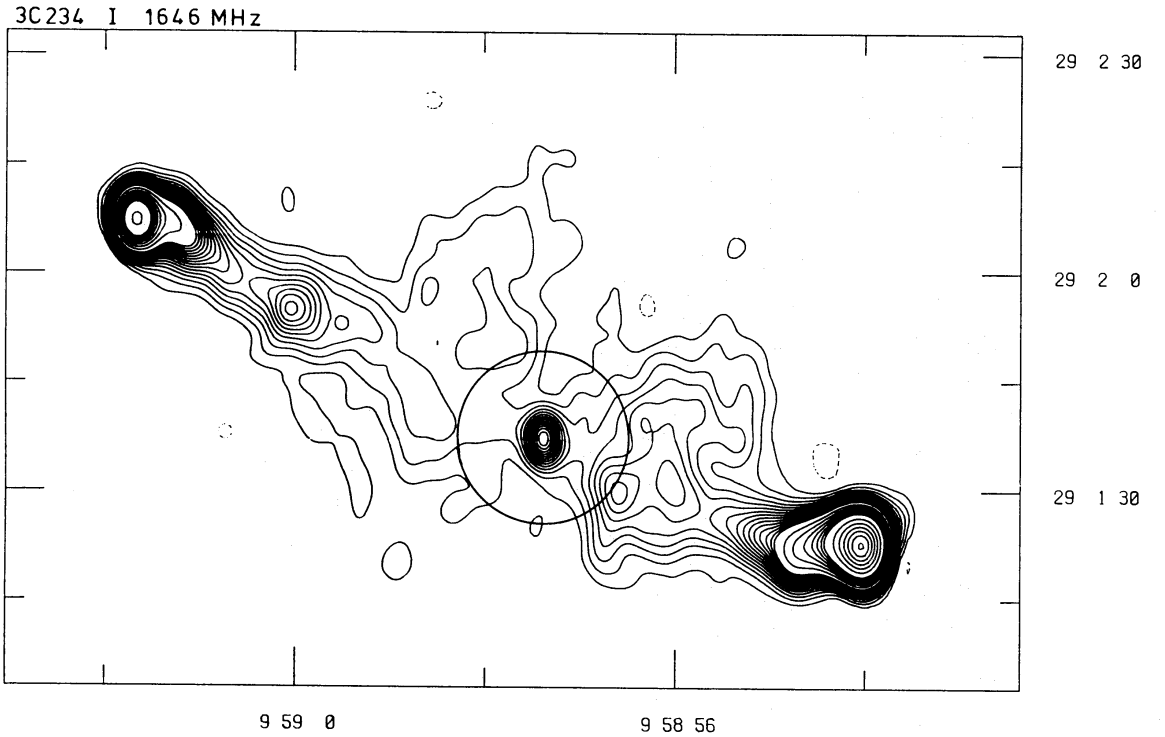

(k)

Figure 2 – *continued*

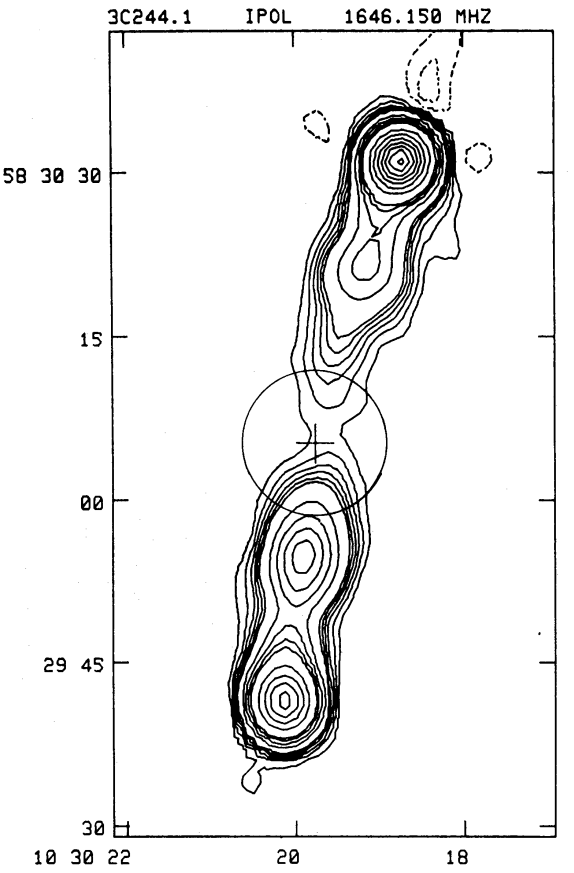

(l)

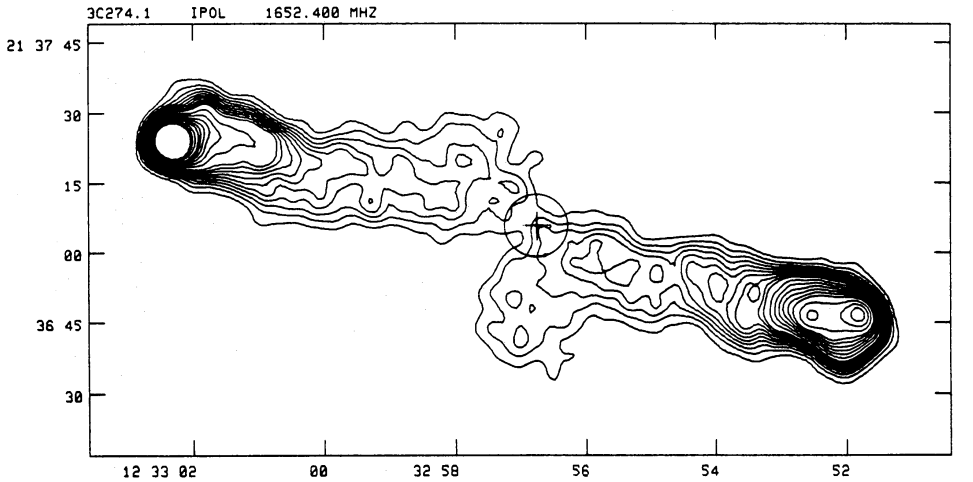

(m)

Figure 2 – *continued*

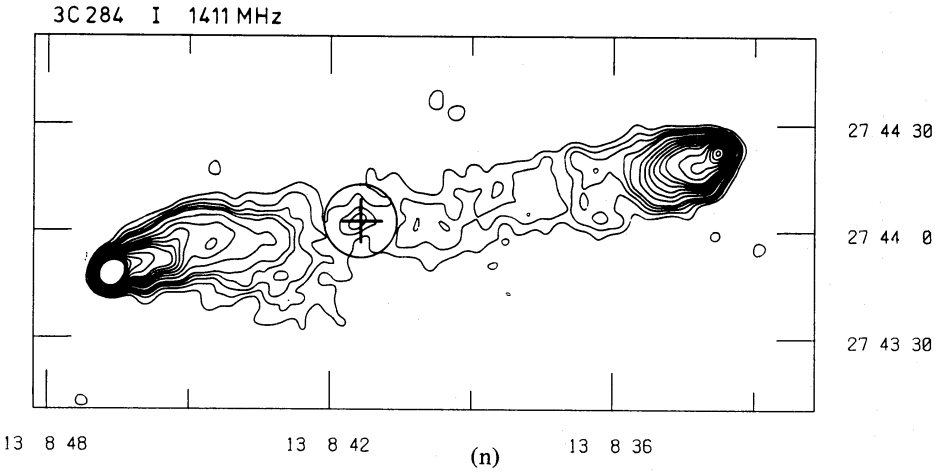

(n)

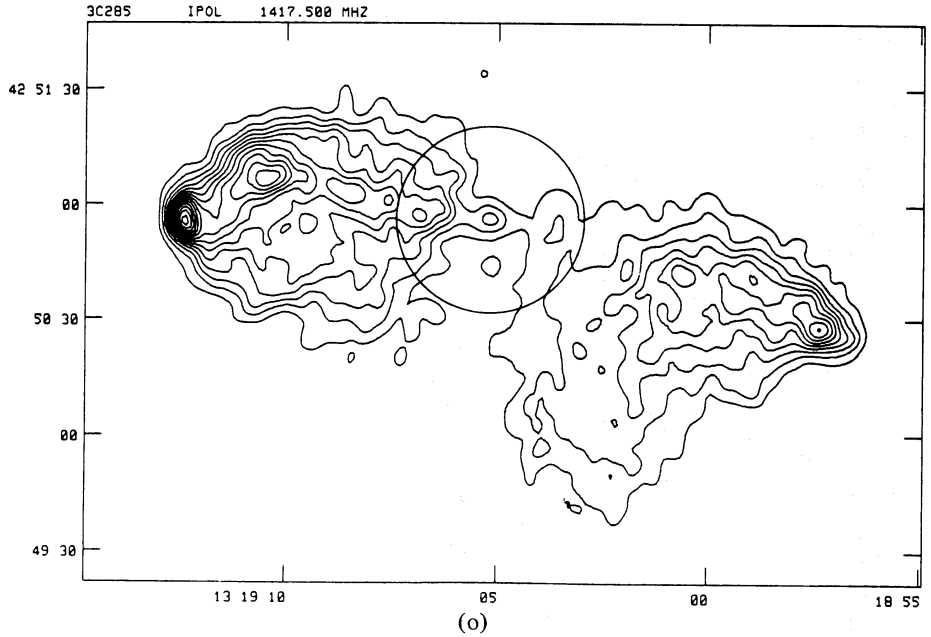

(o)

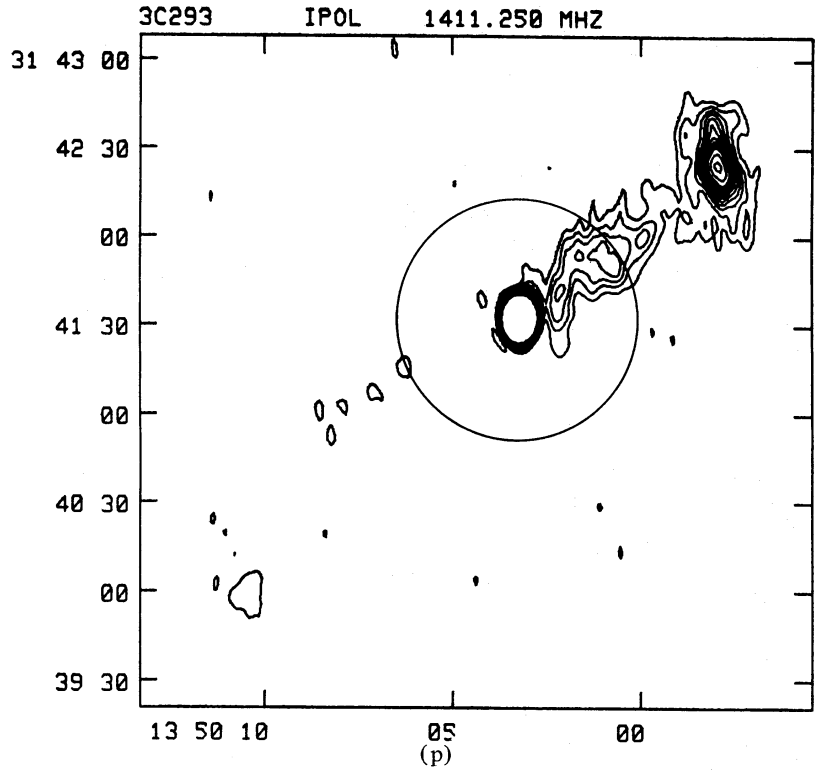

(p)

Figure 2 – *continued*

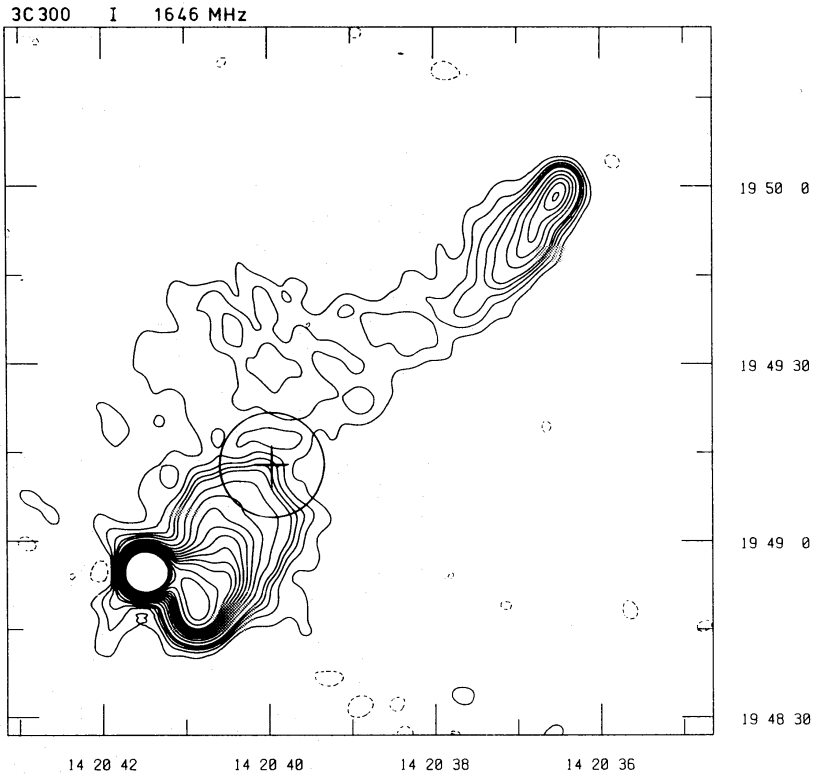

(q)

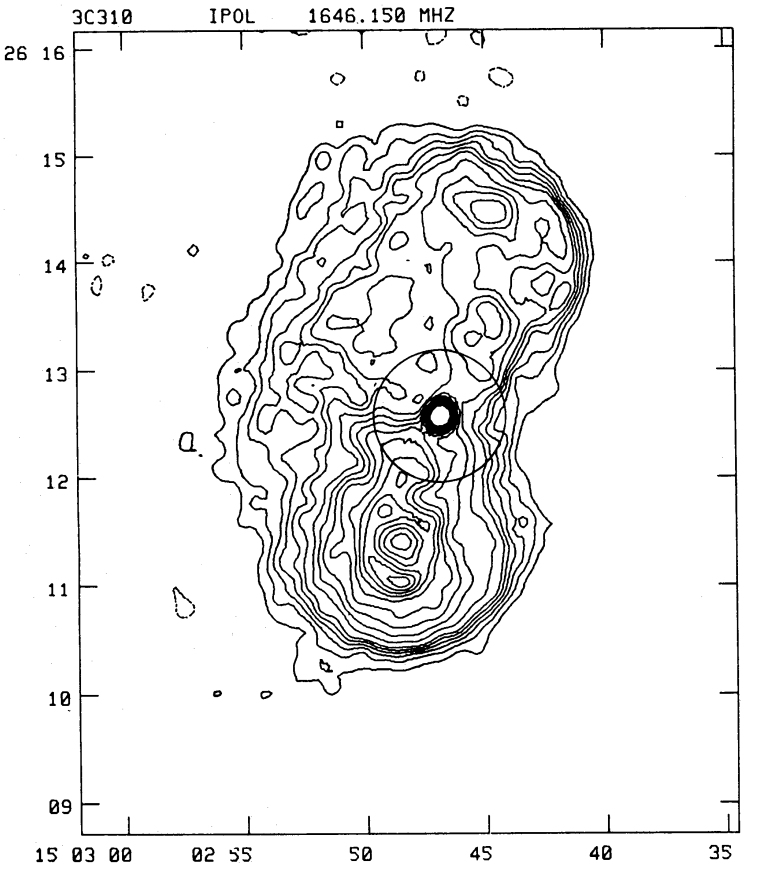

(r)

Figure 2 – *continued*

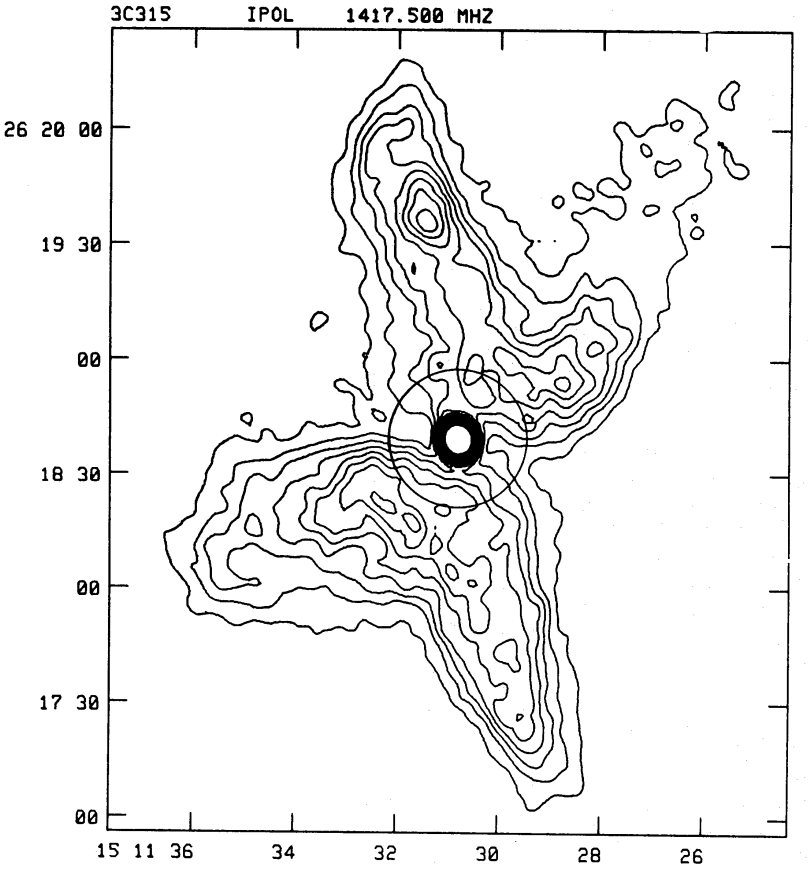

(s)

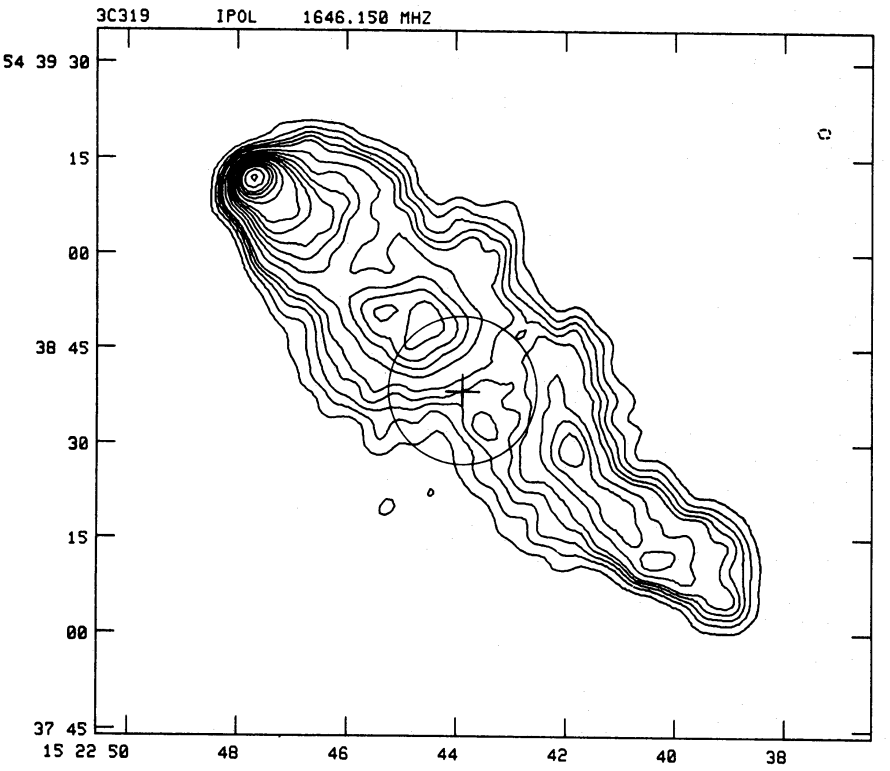

(t)

Figure 2 – *continued*

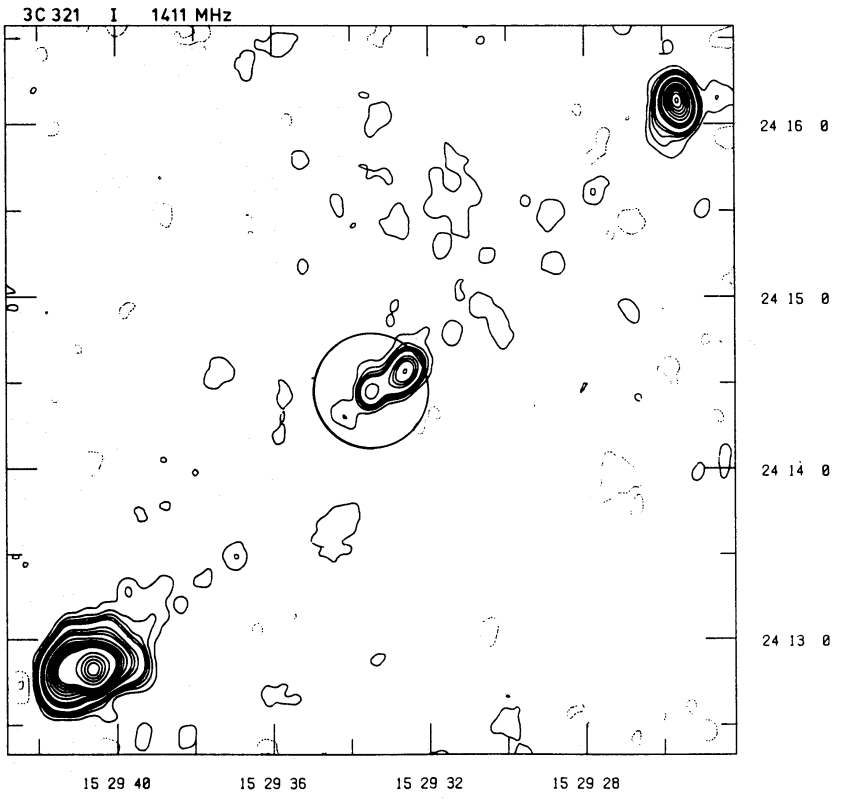

(u)

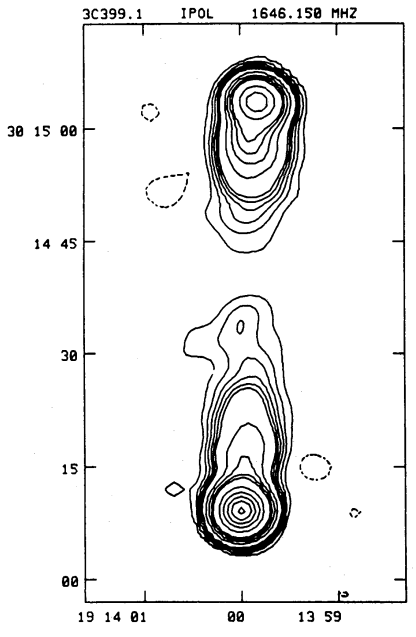

(v)

Figure 2 – *continued*

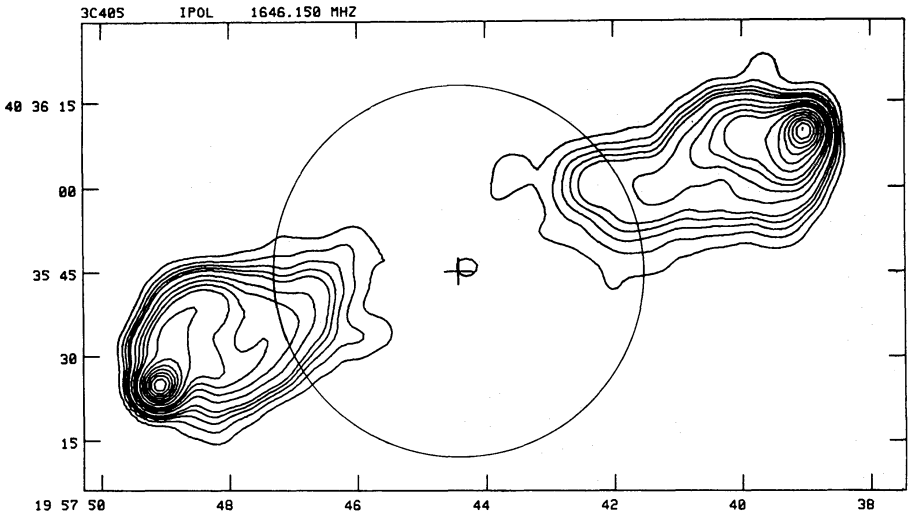

(w)

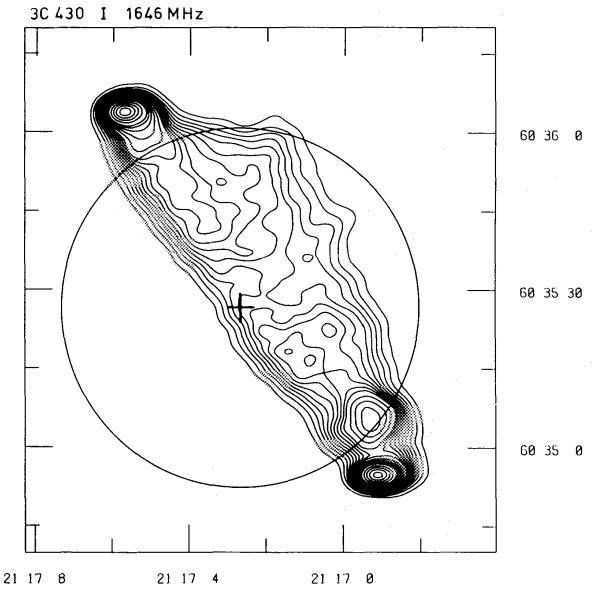

(x)

Figure 2 – *continued*

sometimes omitted. For each identified source a circle of radius 25 kpc has been drawn around the position of the galaxy centre to indicate the extent of a typical giant elliptical galaxy.

For 3C 52, 103 and 165, no redshifts are available for the identifications. We have estimated the V-magnitude of these objects from the Palomar Sky Survey red prints. The reddening towards all three is significant: we have computed A_V using the RC2 formula (de Vaucouleurs & Buta 1983; de Vaucouleurs, de Vaucouleurs & Corwin 1976). We have estimated redshifts from the $V-z$ relation for 3CR radio galaxies (Riley, private communication). The uncertainty in these values is about 50 per cent.

Notes on individual sources follow. Reference is occasionally made to the distortion types listed in Table 5 and discussed in Section 5 below.

(1) 4C 60.02. The larger and fainter of two unrelated sources that contribute to 3C 14.1. The source is unidentified ($b=-2°.3$).

(2) 3C 52. In earlier maps this source appeared to be a good example of a mirror-symmetric distortion, but the structure now appears better described by rotational symmetry. We estimate a redshift of 0.2 from $m_V \simeq 18.5$ (Wyndham 1966); $A_V \simeq 0.7$.

(3) 3C 69. This source is unidentified ($b = 0°.9$). The cross marks the possible central component detected by Pooley & Henbest (1974).

(4) 3C 103. As the only good example of a well-resolved undistorted source, it is interesting that, although the bridge fades near the centre, the actual minimum of brightness is displaced 15 arcsec north of the central component, and the bridge reaches maximum width in the centre (see Fig. 3) in contrast to the simple model by Baldwin (1982), which predicts pinching of the centre of the bridge by the higher pressure near the galaxy. Fomalont (1971) reports a 6-arcmin halo around the source, which may account for a difference of about 10 per cent between the integrated flux of Bridle *et al.* (1972, hereafter BDFL) (after conversion to the Baars *et al.* 1977 scale used here) and the total cleaned flux density at both our observing frequencies. We estimate a redshift of 0.2 from $m_V \simeq 19$ (Macdonald, Kenderdine & Neville 1968) and $A_V \simeq 1.3$.

(5) 3C 111. Nearly half the flux from this well-known double source comes from the highly extended bridge. The emission beyond the Nf hotspot is real. However, because of the brightness contrast between this region and the bridge between the core and the hotspot, we have not included this emission when calculating the axial ratio (Table 1 and Section 5 below).

(6) 3C 134. This source is unidentified ($b = -1°.9$, $A_V \simeq 8$). Observations with the 5-km telescope at 5 GHz show that the bright ridge in the southern lobe has a half-power width of 6 arcsec. If this is a jet, the opening angle ϕ at the nucleus is 5°.

(7) 3C 136.1. Some large-scale structure may be missing from this map, but observations with the one-mile telescope show that the source is not significantly more extended in declination than is shown. The total cleaned flux density at 1415 MHz was 2.86 Jy, consistent with the flux density on the shortest baselines, while BDFL give a total flux density of 3.03 ± 0.24 Jy on the Baars *et al.* (1977) scale.

(8) 3C 139.2. This source is unidentified ($b = -4°.3$). 3C 139.2 has the largest axial ratio in the sample, its total length being nearly 20 times its average width.

(9) 3C 165. 5-km observations at 5 GHz show that the bright ridge in the northern lobe is <2 arcsec in width. The identification (to be discussed in a later paper) is a 19.5-mag red object; $A_V \simeq 0.5$. If this is a galaxy, $z \simeq 0.3$, but it could equally well be a quasar, in which case it is likely to be beyond our redshift limit.

(10) 3C 285. This is the example for type 4 distortion, in which the lobes are bent away from the central galaxy in mirror symmetry. Construction of the half-power plot in Fig. 3 was complicated by the jet in the Nf lobe (mapped here for the first time).

(11) 3C 293. The map shown by Bridle, Fomalont & Cornwall (1981) has better resolution and sensitivity than ours, which we present for completeness. This source is the least luminous in the sample, and differs from normal classical doubles in two respects. First, the ratio of flux density from the two lobes is extreme – other asymmetric sources in our sample have large ratios of peak brightness, but ratios of lobe flux density near one, as found by Macklin (1981) for the 3CR sample. Second, the 'bridge' emission is brighter close to the nucleus and connects directly with it, rather than distorting or fading near the nucleus as in all other sources. The emission visible on our map is superimposed on a fainter bridge visible on the map by Bridle *et al.* The suggestion of Bridle *et al.* that the brighter emission in fact comes from a disrupted jet seems plausible. As in Cen A, Vir A, 3C 236 and 3C 315, the dominating central component is a kpc-scale double extended along the large-scale major axis.

(12) 3C 310. In contrast to 3C 285, this 'fat double' source has no reduction or distortion in the bridge near the galaxy, although the edge of the source nearest the central component is much more sharply defined than the other side (type 5 distortion). The source is identified with the

dominant member of a triplet of galaxies at the centre of a Zwicky cluster. X-ray observations (Burns & Gregory 1982) show that the X-ray structure is bifurcated, with almost as much emission coming from the region of the southern lobe as from the surroundings of the galaxy. Some or all of the latter emission may originate from a point non-thermal source associated with the radio core (Fabbiano *et al.* 1984). Thus the confining medium appears to be associated with the whole cluster rather than being circumgalactic as in most other cases.

(13) 3C 315. The central kpc-scale core is associated with the brighter member of a pair of elliptical galaxies.

(14) 3C 319. The distorted ridges in this source appear to be embedded in a lower-emissivity envelope covering the galaxy. It is thus intermediate between our type 4 and 5 distortions.

(15) 3C 321. This source has a remarkably high compactness for such a low luminosity. The total cleaned flux density at 21 cm is 3.65 Jy, consistent with the flux visible on the longest baselines. The integrated flux density measured by BDFL is 3.69±0.08 Jy at 1412 MHz on the Baars *et al.* (1977) scale, so there is no evidence for any missing flux in our observations. Note that the map has been cleaned well below the faintness contour shown. There is some hint of extended structure in the Np half of the source.

(16) 3C 399.1. This source is unidentified (b=8°.5).

(17) 3C 405 (Cygnus A). On a map with higher dynamic range (Alexander, Brown & Scott 1984), the Sf bridge can be detected all the way in to the nucleus. We used their map to prepare the half-power plot in Fig. 3.

(18) 3C 430. This source is the type example of type 5 distortion. The cocoon is displaced to one side of the source but the edge is sharper on the opposite side, suggesting that the distortion is due to ram pressure. This is consistent with the shape of the hotspots (Burch 1979) and with the displaced X-ray emission (Miller 1983).

5 Discussion

5.1 CENTRAL DISTORTIONS

To investigate the behaviour of bridges close to the associated galaxies, we classified the sources into five types, defined in Table 5. In Fig. 3(a) we give half-power profiles of an example of each type, superimposed on the lowest map contour. The classification of each source is listed in Table 1. Two sources, 3C 293 and 321 have no observed bridge so have not been classified. Note that for the sources 4C 60.02, 3C 69, 244.1 and 399. (all of type 1) the resolution is insufficient to reveal any small distortions such as those seen in 3C 134. The principal result is that less than 30 per cent of our sources have the axisymmetric bridges predicted by simple source models.

Table 5. Source classification.

Type	Description	Example	occurrences
1	No distortion observed in bridge, but marked drop in bridge surface brightness near centre.	3C 103	6
2	Bridge bends away from galaxy only on one side.	3C 284	4
3	Bridge bends away from galaxy into a cross shape. Rotationally symmetric.	3C 274.1	5
4	Both sides of bridge bend away from galaxy in the same direction. Mirror symmetric.	3C 285	4
5	Bridge is continuous across galaxy, which is displaced towards steepest edge of source. Mirror symmetric.	3C 430	3

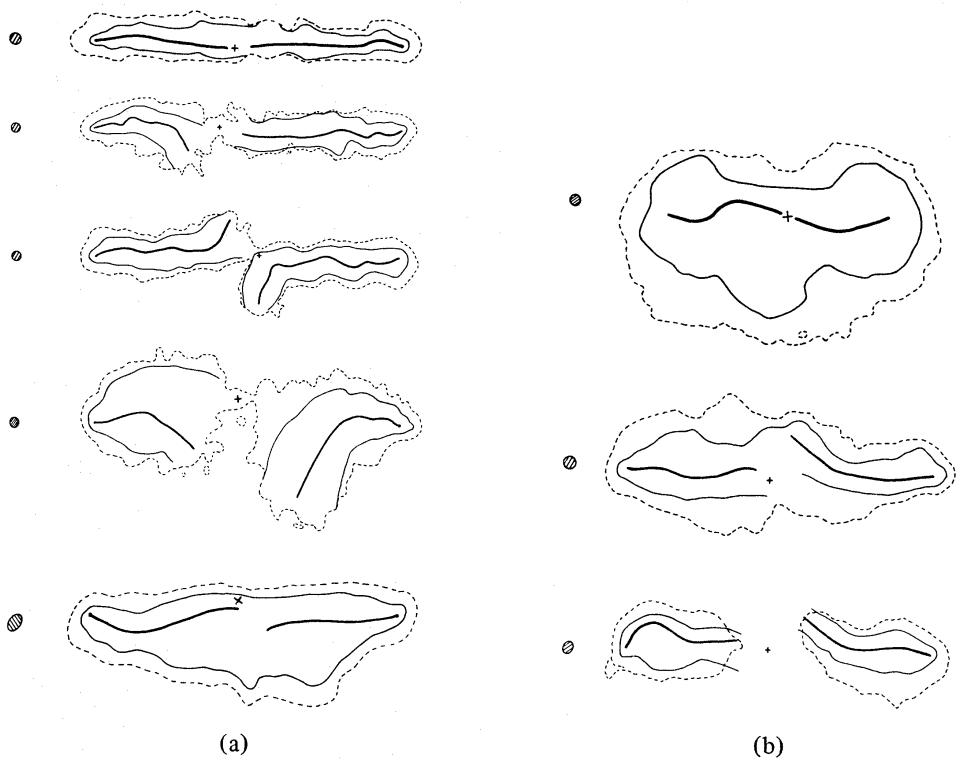

Figure 3. Half-power plots. In each case, a cross marks the central components, a heavy line shows the ridge-line of the bridge, the lighter line marks the half-power width of the source roughly perpendicular to the ridge-line, the dash contour is the lowest contour of the map, and the hatched ellipse gives the beam. (a) Examples of the distortion types listed in Table 5: 3C 103, 284, 274.1, 285 and 430. (b) Examples of sources with complex cross-sections: 3C 310, 319 and 405. The plot of 3C 405 was derived from the map by Alexander *et al.*

An interesting detail is that even in those sources in which the bridge is strongly bent away from the central galaxy (e.g. 3C 285, 315), there is evidence for faint resolved emission across the centre of the source. 3C 319 may be an example in which this emission is of surface brightness comparable to that of the main bridge.

Despite the striking rotational symmetry visible in some of the type 3 sources, we cannot appeal to a model such as that applied to NGC 326 by Ekers *et al.* (1978), in which the symmetry is attributed to the motion of the hotspots at the end of a pair of precessing beams. The characteristic form of the structure observed consists of a straight section along the main axis with a sudden curve near the central galaxy, whereas precession predicts a smooth curve except for particular viewing angles. Furthermore, as Laing (private communication) has pointed out, randomly orientated precessing sources should appear as X-shaped or S-shaped with equal probabilities, whereas only X-shaped sources (our type 3 distortion) are found among FR II objects. Finally, the existence of similar distortions with different symmetries (our types and 2 and 4) suggests a different explanation.

5.2 AXIAL RATIOS

The ratio of length to width (axial ratio) of radio bridges is a fundamental structural parameter which can be directly compared with the predictions of source models. However, no measurements of axial ratios have yet appeared in the literature, primarily because of the difficulties in mapping bridge emission mentioned above. The maps presented in the previous section show that considerable care needs to be taken in defining the 'width' of the bridge. To

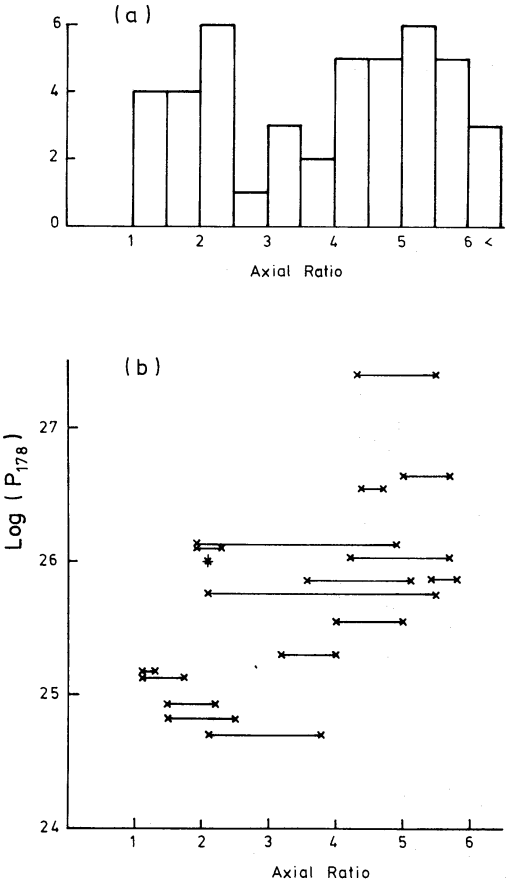

Figure 4. (a) Histogram of axial ratio R for the two ends of all sources. Errors are typically 10–20 per cent by comparing results at 1415 and 1650 MHz. (b) Plot of R against log P_{178} (W Hz^{-1} sr^{-1}) for the identified sources. The values for the two ends of each source are linked.

avoid the complex central regions, we use the width of a section through the bridge half-way between the central component and the outer edge of the source. Well-resolved cross-sections are often asymmetric, and in some cases suggest large-scale emissivity gradients, with a bright central bridge embedded in more diffuse emission. The full width of the section is thus hard to define, and we take the width w as $2/\sqrt{3}$ times the deconvolved half-power width. For a uniformly-emitting elliptical cross-section, w is the full projected width. In Fig. 3(b) we give half-power profiles of three sources (3C 310, 319 and 405) with bridges for which such a simple model is clearly inadequate. In each case the width to the faintest contour is considerably wider than $2/\sqrt{3}$ times the half-power width.

In addition to such large-scale variations, the sections sometimes cross a discrete compact feature such as a recessed hotspot. The half-power was then taken relative to the brightness of the surrounding bridge emission. This was done in 3C 111 (Nf), 3C 134 (Np), 3C 165 (Np), 3C 285 (Nf), and 3C 310 (Sf). The length l is less ambiguous, and is taken as the distance between the nucleus and the outer edge of the source. The axial ratio $R=l/w$ for each end of the source is listed in Table 1, together with the average for the source R_T, defined as $2(l_N+l_S)/(w_N+w_S)$, i.e. the ratio of total length to average width.

In Fig. 4(a), we plot the distribution of axial ratios observed. The distribution is much broader than that expected from projection effects alone. Fig. 4(b) is a plot of the axial ratios against the total power for the identified sources. The correlation of axial ratio with luminosity is highly significant (Spearman Rank Correlation Coefficient $r_s=0.65$ with 17 data points significant at the

1 per cent level). It is worth noting that omitting the three sources with estimated redshifts increases r_s to 0.78 and the significance level to 0.1 per cent. There is no correlation between axial ratio and linear size in our sample.

The trend to increasing axial ratio with luminosity may be physically related to the compactness relation found by Jenkins & McEllin (1977). The expansion speed of the source along its axis is determined by the pressure in the hotspots, while the expansion perpendicular to the axis is probably determined by the bridge pressure. More luminous sources, in which the hotspots tend to be more prominent, are thus expected to have more elongated bridges.

We emphasize that the trend to low axial ratio at low luminosity is followed by sources with well-defined hotspots such as 3C 111 and 430 ('good doubles' in the terminology of Longair & Riley 1979). Thus the compactness and axial ratio relations, which describe the structure of a 'typical' double as a function of luminosity, together predict that low luminosity doubles will frequently have low axial ratios and faint hotspots. Such sources are often treated as a separate class ('wide' or 'fat' doubles), or lumped in with the FR I objects (e.g. Miley 1980), but they appear to be better described as the extreme low-compactness tail of the FR II distribution.

6 Interpretation

6.1 NUMERICAL SIMULATIONS OF THE STANDARD JET MODEL

We performed numerical simulations of the standard jet model of radio sources by integrating the non-relativistic equations of ideal compressible flow using an Eulerian finite-difference method. Further details of the numerical method are given by Williams & Gull (1984). Axisymmetric numerical simulations based on the standard jet model of a radio source typically reveal the main features shown in Fig. 5, which illustrates the flow in a Mach 10 jet propagating into an ambient medium 10 times denser than the jet. The crucial parameter influencing the 'cocoon' of material inflated by the jet is the density ratio between the jet and the confining medium (Norman, Winkler & Smarr 1983; Wilson 1983). If the jet is very much lighter than the confining medium, then, from one-dimensional ram-pressure arguments, the advance speed of the jet-shock is much less than the speed of the jet. A large proportion of the kinetic energy of the jet is therefore converted to thermal energy at the jet-shock, and large quantities of post-jet-shock material flow transversely out of the way of the jet, creating a hotspot somewhat broader than the jet itself and inflating a cocoon. Beyond the radius of the jet, the pressure in the hotspot, which is not balanced by the ram-pressure of the jet, re-accelerates the post-jet-shock material towards the centre, producing backflow. Conversely, if the jet density is greater than the material on which it impinges, then relatively little energy is lost, and the ex-jet material continues to move forwards in a 'lump' trailing behind the jet-shock. Heavy jets therefore do not produce cocoons, strong hotspots or backflow.

Whereas in the simulations of Norman *et al.* the backflow is allowed to flow off the computing grid in the central plane, effectively modelling the end of a long jet, we wish to model the boundary conditions more appropriate to a classical double ratio source, in which it is clear that the backflow cannot continue indefinitely from both hotspots. Following Wilson, we have therefore imposed a symmetry plane through the nucleus. The backflow then remains collimated until it reaches the source galaxy where it meets the backflow from the opposite hotspot and, under the enforced axisymmetry of our simulations, expands laterally in a fat disc (see Fig. 5). We show below that we expect the disc to be unstable to non-axisymmetric perturbations.

It is not clear how to associate these theoretical structures with the observed radio emission. To generate the synchrotron emission we require magnetic fields with energy density several times higher than the possible thermal energy density in the gaseous haloes surrounding radio galaxies (Miller 1983), together with a similar energy density in relativistic particles. Both of these can be

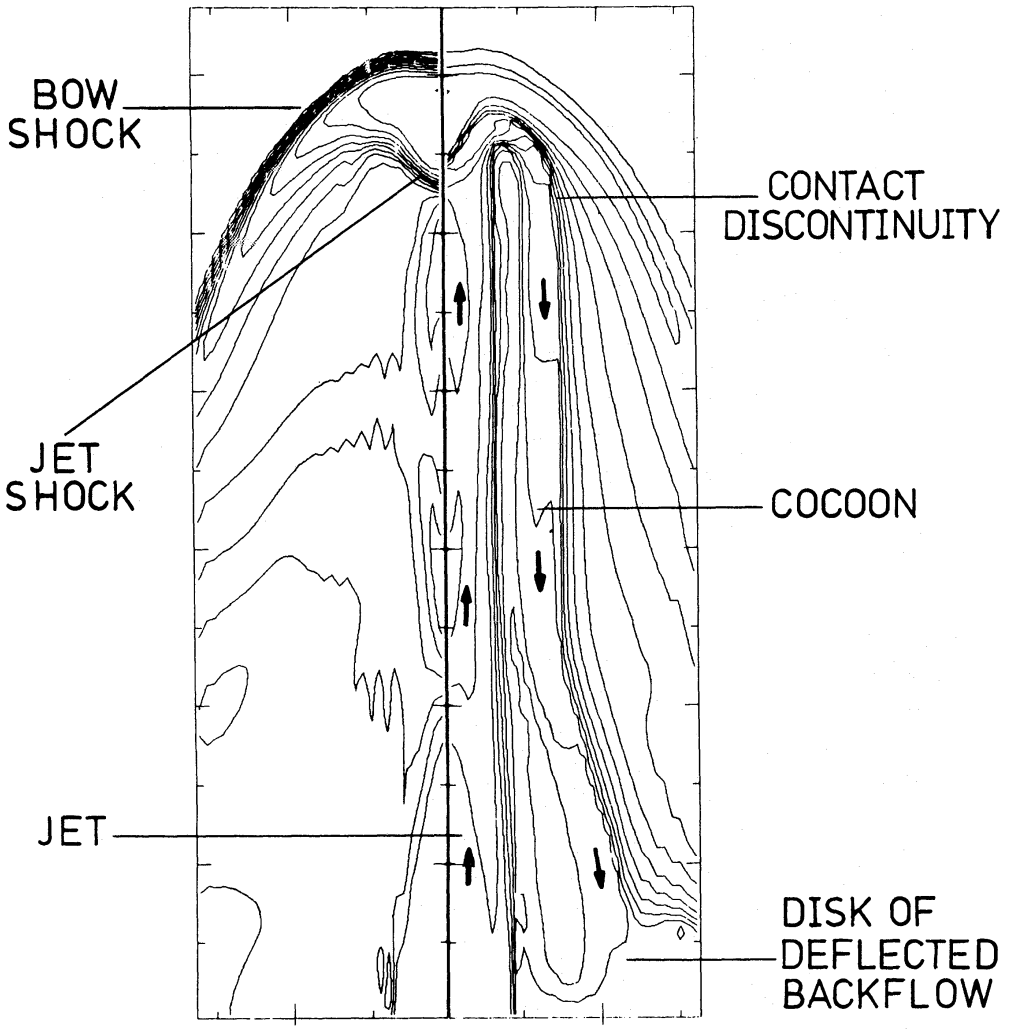

Figure 5. Numerical simulation of a classical double radio source. The left half of the diagram displays pressures and the right half density. In each half the contour interval is logarithmic and there are fourteen contours between the data maximum and minimum. In this axisymmetric model the lower boundary is impermeable in order to simulate the effect mirror symmetry in the source. Density contrast between the jet and the external medium is 0.1; internal Mach number of the jet is 10.

generated by strong shocks and turbulence. Clearly, all the material in the cocoon has passed through such a region, but the bow shock is also strong, especially near the hotspots, and turbulence in the shocked confining medium is possible, especially if the contact discontinuity is unstable. To model the radio emission expected from the hotspots, Wilson & Scheuer (1983) allowed their bow-shock to produce relativistic particles and, by implication, magnetic fields. A priori it is equally plausible, however, to assume that the necessary seed population of mildly relativistic particles and magnetic fields is only present in the jet material, giving rise to emission only within the contact discontinuty. The distortions observed in the bridges of our sample suggest furthermore that, far from the hotspots at least, the bow-shock (which we would expect to remain roughly ellipsoidal) is not a significant source of relativistic particles. We therefore assume that radio emission in the bridge comes only from material inside the contact discontinuity. An apparent problem with interpreting the contact discontinuity as the edge of the bridge is that, whereas most maps show bridges which are much wider than the size of the hotspot, the width of the cocoon in simulations is only a few times that of the jet. We believe, however, that

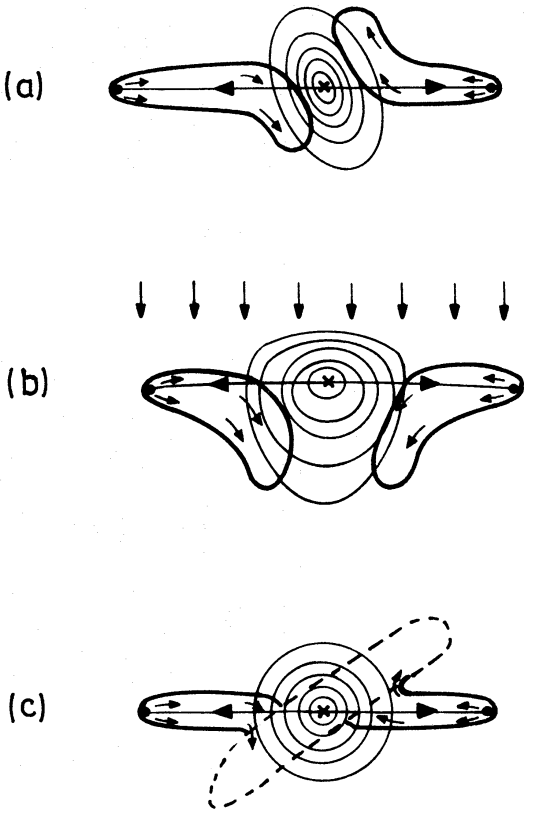

Figure 6. Sketch diagrams of the three symmetry-breaking mechanisms discussed in the text. Each diagram shows the expected X-ray contours (thin lines), the radio core (x), the outline of the radio source (thick line), and arrows giving the flow pattern. (a) Non-aligned spheroidal gas distribution; type 2 distortion. (b) Galaxy in motion (heavy arrows illustrate 'wind of passage'); type 3 distortion. (c) Old cavity (dashed outline) channels backflow. Type 2 distortion.

axisymmetric simulations underestimate the width of the cocoon, because the jet direction in real sources may vary as in the 'Dentist's Drill' model (Scheuer 1982). In addition, astrophysical jets may be considerably more diffuse than those so far simulated and therefore produce broader cocoons.

6.2 BRIDGE DISTORTIONS NEAR GALAXIES

Baldwin (1982) has emphasized the importance of the variation in density of the confining medium on the shape of radio sources. In our numerical simulations, due to limitations in computing resources, we assume that the external medium has constant density and pressure, and that there is axial symmetry. Clearly, the predicted shape of the disc of emission depends strongly upon these assumptions. Relaxing the first assumption will pinch-off the central bulge near the nucleus and deflect the backflow earlier because of the thermal pressure gradient away from the nucleus. Breaking the axial symmetry changes the problem more fundamentally: rather than widening suddenly, we expect the backflow to follow the path of least resistance and, in the thoroughly asymmetric case, produce a bridge bent away from the galaxy. In general, some widening of the bridge may occur, but the flow will be strongest in some particular direction.

We suggest three possible symmetry-breaking mechanisms:

(1) The source axis is not parallel to the axis of a spheroidal gas distribution surounding the galaxy. This gives rise to a type 3 distortion. More generally, an irregular gas distribution will

deflect each half of the bridge in an independent direction, giving rise to equal numbers of types 3 and 4 sources, with type 2 sources where the line-of-sight is such that one of the bent bridges is projected across the galaxy.

(2) Motion of the source galaxy through the surrounding intergalactic medium creates a ram-pressure gradient across the bridge, and also distorts the gaseous halo of the galaxy into an egg-shape. Both effects favour a type 4 distortion.

(3) If the source axis has varied considerably in the past, the old cocoon provides a channel into which the backflow from the new bridge may be deflected. Such a mechanism may explain the extreme distortions in 3C 315 and 52.

Fig. 6 illustrates these three mechanisms. Since the jet must contain material less dense than the IGM in order to inflate a cocoon, we expect that any distortion in the bridge will be amplified by the effects of buoyancy. None of these mechanisms accounts well for the type 5 distortion since, in each case, the bridge is expected to avoid the central object, whereas in type 5 sources the central object does not noticeably affect the bridge. It is clear that some type 5 objects are simply sources close to the line-of-sight, so that the central object is projected on to a normal distorted bridge. A second possibility is that the density of the confining medium varies too slowly over the bridge to have much effect. This may be the case for 3C 430, the smallest source in the sample. For 3C 310, as suggested above, the radio source may be confined by the cluster atmosphere rather than gas associated with the source galaxy. Similar comments apply to sources of type 1, which may simply be the higher-luminosity equivalent of type 5.

The mechanisms suggested for breaking the symmetry of the standard model can be used to make tentative predictions about the distributions of hot gas surrounding radio sources. Unfortunately, although many of the sources discussed have been observed with the *Einstein* satellite (e.g. Fabbiano *et al.* 1984), the resolution and sensitivity available are not yet sufficient to map the gas distribution surrounding most 3C classical doubles.

7 Conclusions

We have mapped the bridge emission in a complete sample of classical double radio sources with $z<0.5$ and $\theta>45$ arcsec. We find that

(1) in at least 60 per cent of our sources, the bridge is distorted away from the central axis near the centre, on one or both sides. Comparisons with numerical simulations of supersonic jets suggest that this distortion is an expected consequence of the interaction between the strong backflow, which occurs when the jets are less dense than the confining medium, and the galactic atmosphere;

(2) axial ratio is correlated with luminosity between $P_{178}=5\times10^{24}$ and 5×10^{26} W Hz^{-1} sr^{-1}, rising from 1–2 to about 5. This effect is probably caused by the increased pressure difference between the hotpots and the bridge in higher luminosity sources, which is implied by the compactness relation of Jenkins & McEllin (1977).

Acknowledgments

JPL thanks the staff of the VLA for their hospitality and help during the observations and data reduction. We are grateful to Guy Pooley for helping with data reduction. We thank Paul Alexander for allowing us to use his map of Cygnus A, and Mike Wilson and Steve Gull for helpful discussions. We thank Irena Tabecka for her expert draughtsmanship. The VLA is operated by the National Radio Astronomy Observatory for Associated Universities, Inc., under contract from the National Science Foundation. The numerical simulations were performed on

the SERC STARLINK node at Cambridge. We are both supported by SERC research studentships.

References

Alexander, P., Brown, M. T. & Scott, P. F., 1984. *Mon. Not. R. astr. Soc.,* **209,** 851.

Baars, J. W. M., Genzel, R., Pauliny-Toth, I. I. K. & Wetzel, A., 1977. *Astr. Astrophys.,* **61,** 99.

Baldwin, J. E., 1982. *Extragalactic Radio Sources, IAU Symp. 97,* p. 21, eds Heeschen, D. S. & Wade, C. M., Reidel, Dordrecht, Holland.

Bridle, A. H. & Fomalont, E. B., 1979. *Astr. J.,* **84,** 1679.

Bridle, A. H., Davis, M. M., Fomalont, E. B. & Lequeux, J., 1972. *Astr. J.,* **77,** 405.

Bridle, A. H., Fomalont, E. B. & Cornwall, T. J., 1981. *Astr. J.,* **86,** 1294.

Burch, S. F., 1979. *Mon. Not. R. astr. Soc.,* **186,** 293.

Burns, J. O. & Gregory, S. A., 1982. *Astr. J.,* **87,** 1245.

de Vaucouleurs, G. H. & Buta, R., 1983. *Astr. J.,* **88,** 939.

de Vaucouleurs, G. H., de Vaucouleurs, A. & Corwin, H. G., 1976. *Second Reference Catalogue of Bright Galaxies,* University of Texas Press, Austin.

Ekers, R. D., Fanti, R., Lari, C. & Parma, P., 1978. *Nature,* **276,** 588.

Fabbiano, G., Miller, L., Trinchieri, G., Longair, M. & Elvis, M., 1984. *Astrophys. J.,* **277,** 115.

Fanaroff, B. L. & Riley, J. M., 1974. *Mon. Not. R. astr Soc.,* **167,** 31P.

Fomalont, E. B., 1971. *Astr. J.,* **76,** 513.

Fomalont, E. B. & Bridle, A. H., 1983. *The AIPS Cookbook,* National Radio Astronomy Observatory, Charlottesville.

Jenkins, C. J. & McEllin, M., 1977. *Mon. Not. R. astr. Soc.,* **180,** 219.

Jenkins, C. J., Pooley, G. G. & Riley, J. M., 1977. *Mem. R. astr. Soc.,* **84,** 61.

Laing, R. A., Riley, J. M. & Longair, M. S., 1983. *Mon. Not. R. astr. Soc.,* **204,** 151.

Longair, M. S. & Riley, J. M., 1979. *Mon. Not. R. astr. Soc.,* **188,** 625.

Macdonald, G. H., Kenderdine, S. & Neville, A. C., 1968. *Mon. Not. R. astr. Soc.,* **138,** 259.

Macklin, J. T., 1981. *Mon. Not. R. astr. Soc.,* **196,** 967.

Miley, G. K., 1980. *Ann. Rev. astr. Astrophys.,* **18,** 165.

Miller, L., 1983. *PhD thesis,* University of Cambridge.

Norman, M. L., Winkler, K.-H. A. & Smarr, L., 1983. *Astrophysical Jets,* p. 227, eds Ferrari, A. & Pacholczyk, A. G., Reidel, Dordrecht, Holland.

Peacock, J. A. & Wall, J. V., 1981. *Mon. Not. R. astr. Soc.,* **194,** 331.

Pooley, G. G. & Henbest, S. N., 1974. *Mon. Not. R. astr. Soc.,* **169,** 477.

Riley, J. M. & Pooley, G. G., 1975. *Mem. R. astr. Soc.,* **80,** 105.

Scheuer, P. A. G., 1982. *Extragalactic Radio Sources, IAU Symp. 97,* p. 163, ed. Heeschen, D. S. & Wade, C. M., Reidel, Dordrecht, Holland.

Schwab, F., 1980. *Proc. Soc. photo-opt. Instrum. Engng.,* **231,** 18.

Scott, P. F., 1982. *Extragalactic Radio Sources, IAU Symp. 97,* p. 29, eds Heeschen, D. S. & Wade, C. M., Reidel, Dordrecht, Holland.

Spangler, S. R. & Bridle, A. H., 1982. *Astr. J.,* **87,** 1270.

Thompson, A. R., Clark, B. G., Wade, C. M. & Napier, P. J., 1980. *Astrophys. J. Suppl.,* **44,** 151.

van Breugel, W. J. M. & Fomalont, E. B., 1984. *Astrophys. J.,* in press.

Williams, A. G. & Gull, S. F., 1984. *Nature,* **310,** 33.

Wilson, M. J., 1983. *PhD thesis,* University of Cambridge.

Wilson, M. J. & Scheuer, P. A. G., 1983. *Mon. Not. R. astr. Soc.,* **205,** 449.

Wyndham, J. D., 1966. *Astrophys. J.,* **144,** 459.